Astroparticle Physics 158 (2024) 102945

Contents lists available at ScienceDirect

Astroparticle Physics

journal homepage: www.elsevier.com/locate/astropartphys

Alpha backgrounds in NaI(Tl) crystals of COSINE-100

G. Adhikari [a], N. Carlin [b], D.F.F.S. Cavalcante [b], J.Y. Cho [c], J.J. Choi [c,d], S. Choi [d], A.C. Ezeribe [e], L.E. França [b], C. Ha [f], I.S. Hahn [h,g,i], S.J. Hollick [a], E.J. Jeon [c,i,*], H.W. Joo [d], W.G. Kang [c], M. Kauer [j,*], B.H. Kim [c], H.J. Kim [k], J. Kim [f], K.W. Kim [c], S.H. Kim [c], S.K. Kim [d], S.W. Kim [c], W.K. Kim [c,i], Y.D. Kim [c,i,l], Y.H. Kim [c,m,i], Y.J. Ko [c], D.H. Lee [k], E.K. Lee [c], H. Lee [c,i,*], H.S. Lee [c,i], H.Y. Lee [g], I.S. Lee [c], J. Lee [c], J.Y. Lee [k], M.H. Lee [c,i], S.H. Lee [c,i], S.M. Lee [d], Y.J. Lee [f], D.S. Leonard [c], N.T. Luan [k], B.B. Manzato [b], R.H. Maruyama [a], R.J. Neal [e], J.A. Nikkel [a], S.L. Olsen [c], B.J. Park [c,i], H.K. Park [n], H.S. Park [m], J.C. Park [o], K.S. Park [c], S.D. Park [k], R.L.C. Pitta [b], H. Prihtiadi [p], S.J. Ra [c], C. Rott [q,r], A. Scarff [e], K.A. Shin [c], M.K. Son [o], N.J.C. Spooner [e], L.T. Truc [k], L. Yang [s], G.H. Yu [c,q,*], COSINE-100 Collaboration

[a] *Department of Physics and Wright Laboratory, Yale University, New Haven, CT 06520, USA*
[b] *Physics Institute, University of São Paulo, 05508-090, São Paulo, Brazil*
[c] *Center for Underground Physics, Institute for Basic Science (IBS), Daejeon 34126, Republic of Korea*
[d] *Department of Physics and Astronomy, Seoul National University, Seoul 08826, Republic of Korea*
[e] *Department of Physics and Astronomy, University of Sheffield, Sheffield S3 7RH, United Kingdom*
[f] *Department of Physics, Chung-Ang University, Seoul 06973, Republic of Korea*
[g] *Center for Exotic Nuclear Studies, Institute for Basic Science (IBS), Daejeon 34126, Republic of Korea*
[h] *Department of Science Education, Ewha Womans University, Seoul 03760, Republic of Korea*
[i] *IBS School, University of Science and Technology (UST), Daejeon 34113, Republic of Korea*
[j] *Department of Physics and Wisconsin IceCube Particle Astrophysics Center, University of Wisconsin-Madison, Madison, WI 53706, USA*
[k] *Department of Physics, Kyungpook National University, Daegu 41566, Republic of Korea*
[l] *Department of Physics, Sejong University, Seoul 05006, Republic of Korea*
[m] *Korea Research Institute of Standards and Science, Daejeon 34113, Republic of Korea*
[n] *Department of Accelerator Science, Korea University, Sejong 30019, Republic of Korea*
[o] *Department of Physics and IQS, Chungnam National University, Daejeon 34134, Republic of Korea*
[p] *Department of Physics, Universitas Negeri Malang, Malang 65145, Indonesia*
[q] *Department of Physics, Sungkyunkwan University, Suwon 16419, Republic of Korea*
[r] *Department of Physics and Astronomy, University of Utah, Salt Lake City, UT 84112, USA*
[s] *Department of Physics, University of California San Diego, La Jolla, CA 92093, USA*

ARTICLE INFO

Keywords:
NaI(Tl)
^{210}Pb
^{210}Po
^{232}Th
^{216}Po
Half-life
Alpha
Quenching

ABSTRACT

COSINE-100 is a dark matter direct detection experiment with 106 kg NaI(Tl) as the target material. ^{210}Pb and daughter isotopes are a dominant background in the WIMP region of interest and are detected via β decay and α decay. Analysis of the α channel complements the background model as observed in the β/γ channel. We present the measurement of the quenching factors and Monte Carlo simulation results and activity quantification of the α decay components of the COSINE-100 NaI(Tl) crystals. The data strongly indicate that the α decays probabilistically undergo two possible quenching factors but require further investigation. The fitted results are consistent with independent measurements and improve the overall understanding of the COSINE-100 backgrounds. Furthermore, the half-life of ^{216}Po has been measured to be 143.4 ± 1.2 ms, which is consistent with and more precise than most current measurements.

* Corresponding authors.
E-mail addresses: ejjeon@ibs.re.kr (E.J. Jeon), mkauer@physics.wisc.edu (M. Kauer), gksmrf222333@naver.com (H. Lee), tksxk752@naver.com (G.H. Yu).

https://doi.org/10.1016/j.astropartphys.2024.102945
Received 9 November 2023; Received in revised form 30 January 2024; Accepted 8 February 2024
Available online 9 February 2024

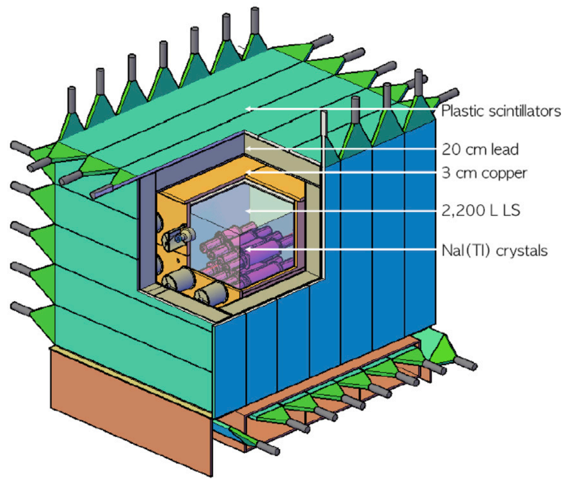

Fig. 1. COSINE-100 detector geometry implemented in Geant4 (Section 4).

1. Introduction

The COSINE-100 detector consists of an array of eight ultra-pure NaI(Tl) crystals with a combined mass of 106 kg. The experiment was operated at the Yangyang Underground Laboratory (Y2L) from September 2016 until March 2023. Its primary goal is the direct detection of dark matter via the annual modulation of WIMP scattering from I or Na nuclei. The crystal array is immersed in 2200 liters of liquid scintillator for background tagging.

A good understanding and precise measurement of the background sources contributing events in the 1–10 electron-equivalent keV (keV_{ee}) region of interest (ROI) is critical to NaI(Tl) direct detection WIMP searches. Bulk and surface ^{210}Pb are the dominant background sources in this region and are observed in the β/γ channel, as well as in the α channel. Certain characteristics (gain calibration, energy resolution, light yield, etc.) of the NaI crystals have been measured in situ [1]. The quenching factors for α particles are important inputs to the simulation, as well as the analysis of the α background. Analysis of the α channel can improve the accuracy of the background model in the ROI. Analysis of the α backgrounds using 2.7 yr data is presented in this work, intended to quantify the activity of the different components by fitting data using Monte Carlo simulations and a direct determination of quenching factors for alpha particles.

2. COSINE-100 experimental setup

The experimental setup and data acquisition are described in detail in Ref. [1,2]. The detector geometry used for simulations is shown in Fig. 1. Eight NaI(Tl) crystals (denoted C1–C8), arranged in two layers, are located in the middle of a four-layer shielding structure. From outside inward, the four shielding layers are plastic scintillator panels, a lead-brick castle, a copper box, and a scintillating liquid. The eight NaI(Tl) crystal assemblies and their support table are immersed in the scintillating liquid that serves both as an active veto and a passive shield [3,4].

The eight NaI(Tl) crystals were grown out of batches of powder provided by Alpha Spectra Inc. with successive improvements. The first crystals labeled AS-B and AS-C were produced with a reduction of ^{40}K by an order of magnitude compared to crystals grown with AS-A powder. Then, crystals labeled WIMPScint-II (AS-WSII) reduced the contamination of ^{210}Pb. Finally, the crystals labeled WIMPScint-III (AS-WSIII) were produced with an additional reduction of ^{40}K by a factor of two. The crystal properties are summarized in Table 1, and a detailed description is given in Ref. [1].

Table 1
COSINE-100 crystal properties. The total α rates were independently measured as part of the crystal commissioning effort. Details of the measurements are described in Ref. [1].

NaI (Tl) Crystal	Mass (kg)	Size (inches) (diam. ×length)	Powder Type	Total α rate (mBq/kg)	^{40}K (ppb)
C1	8.3	5.0 x 7.0	AS-B	3.20 ± 0.08	34.7 ± 4.7
C2	9.2	4.2 x 11.0	AS-C	2.06 ± 0.06	60.6 ± 4.7
C3	9.2	4.2 x 11.0	AS-WSII	0.76 ± 0.02	34.3 ± 3.1
C4	18.0	5.0 x 15.3	AS-WSII	0.74 ± 0.02	33.3 ± 3.5
C5	18.3	5.0 x 15.5	AS-C	2.06 ± 0.05	82.3 ± 5.5
C6	12.5	4.8 x 11.8	AS-WSIII	1.52 ± 0.04	16.8 ± 2.5
C7	12.5	4.8 x 11.8	AS-WSIII	1.54 ± 0.04	18.7 ± 2.8
C8	18.3	5.0 x 15.5	AS-C	2.05 ± 0.05	54.3 ± 3.8

The final crystals are cylindrically shaped and hermetically encased in OFE copper tubes with wall thickness of 1.5 mm and quartz windows (12.0 mm thick) at each end. Each crystal's lateral surface is wrapped in roughly 10 layers of 250 μm thick PTFE reflective sheets. The quartz windows are optically coupled to each end of the crystal via 1.5 mm thick optical pads. These, in turn, are optically coupled to 3-inch Hamamatsu R12669SEL photomultiplier tubes (PMTs) with a thin layer of high-viscosity optical gel. The PMTs are sealed from the liquid scintillator by a housing made of copper and PTFE.

It should be noted that Crystal-5 and Crystal-8 are excluded from this work due to significant degradation of the light collection.

The scintillation signals are digitized and integrated to determine the charge in arbitrary units. Special calibration runs and prominent peaks from in situ data are used to define the calibration function [2] that converts the digitized charge into units of electron-volts (eV). The calibration function is determined from the β/γ scintillation signals and is referred to as the electron-equivalent energy (eV_{ee}).

3. Alpha quenching measurements

The α events are selected from data using the meantime variable as discussed in Section 3.1. The observed energy of the α events is used to build the energy spectra. The energy spectra are in units of electron-equivalent energy and do not represent the true α energy. Only a fraction of the α decay energy is converted to light. The ratio of the observed energy to the decay energy is referred to as the α quenching factor (QF). To determine the crystal quenching factors, known α peaks are identified in data as described in Section 3.2. The quenching factor is also α energy dependent so ideally multiple known α peaks are required to determine the energy dependent quenching factor function as summarized in Section 3.3.

3.1. Alpha event selection and energy spectra

The scintillation signal from α particles in NaI(Tl) differs from the one generated by β/γ particles. The decay time of the scintillation pulse by α is faster than the one from β/γ particles. The scintillation decay time of the incident particles can be identified from the charge-weighted duration time, called the meantime. The meantime $\langle t\rangle$ is defined as

$$\langle t\rangle = \frac{\Sigma_i A_i t_i}{\Sigma_i A_i}, \tag{1}$$

where A_i and t_i are the charge and time of the i-th digitized bin of a signal waveform, respectively. The meantime is estimated in COSINE-100 data within 1.5 μs from the pulse start time. As a result, the populations of β/γ events and α events are clearly separated due to the faster decay times of the α-induced events as shown in Fig. 2.

Using the meantime selection criteria, the α events are selected from data. We obtain the α energy spectra in units of electron-equivalent energy (keV_{ee}) as shown in Fig. 3. The half-lives of the two prominent peaks are consistent with ^{210}Po. The ANAIS experiment observed two

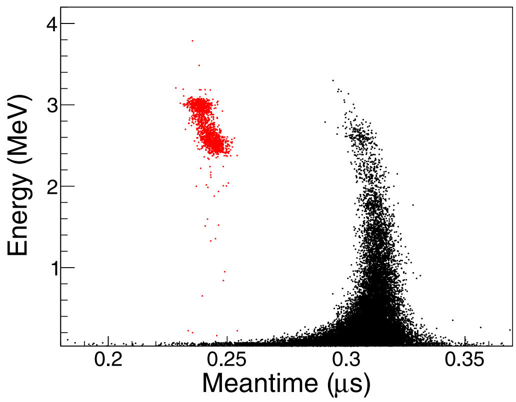

Fig. 2. Typical crystal scatter plot of the meantime versus the energy for COSINE-100 background data shown for crystal C6 as an example. The α events (red dots) and the β/γ events (black dots) are clearly identified by the meantime as defined by Eq. (1).

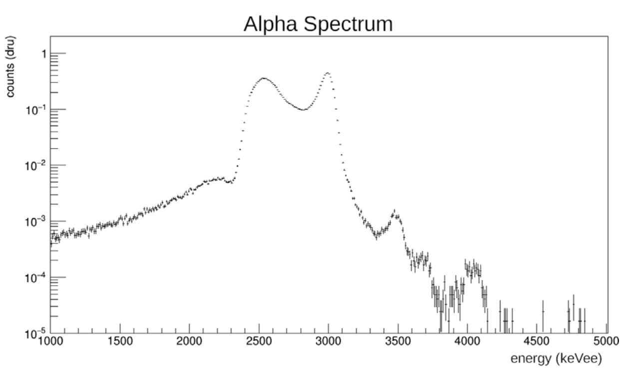

Fig. 3. Characteristic electron-equivalent energy spectrum of α events shown for crystal C6 as an example. ^{210}Po makes up the two prominent peaks suggesting two quenching factors.

prominent peaks in their alpha spectra [5] and cautiously proposes surface ^{210}Po as an explanation. Discussed in detail in Section 4, MC simulation of surface ^{210}Po was insufficient to explain the two peak structure observed in our data. A recent preliminary study by the COSINUS experiment [6] may provide stronger evidence of QF dependence on Tl doping concentration once the study matures. In principle, the NaI(Tl) crystal growing processes can cause spatial dependence of the Tl doping concentration within the crystal. The spatial dependence of the QF could be a continuum, distinctly different, or a combination of both. In this work, we consider two different quenching factors for α events. The high QF and low QF are referred to as Q_1 and Q_2 respectively.

3.2. Alpha-alpha time-correlated events

The high energy region ($> 3.3\,\mathrm{MeV}_{ee}$) of the α distribution, as shown in Fig. 3, is from the ^{228}Th-group α decays and more specifically from ^{220}Rn and ^{216}Po. The ^{228}Th-group activity can be measured by selecting the time-delayed α-α events from ^{220}Rn and ^{216}Po decays. The α decay of ^{216}Po has a short half-life of 0.145 s following its production via the α decay of ^{220}Rn.

The ^{228}Th-group activity can be calculated from a single exponential fit to the α-α time-delay (ΔT) distribution. Events with ΔT greater than 5 s are rejected. A typical ΔT distribution and fitted function is shown in Fig. 4 and the fitted half-lives of all crystals are summarized in Table 2.

It should be noted that our measured average ^{216}Po half-life of 143.4 ± 1.2 ms is very competitive with the leading measurements [7–11]. This measurement is more precise than previous measurements with the exception of [8]. Previous ^{216}Po half-life measurements are listed in Table 3 for comparison.

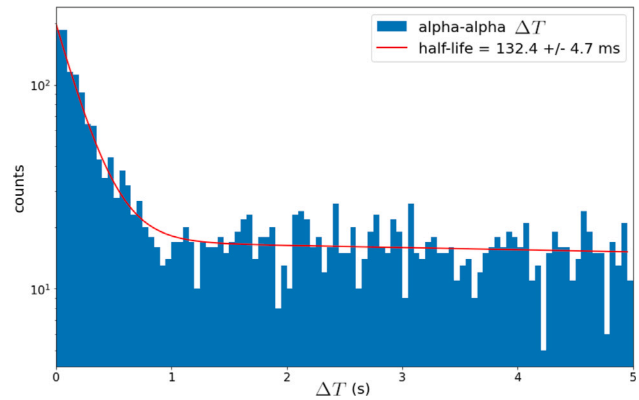

Fig. 4. A typical ΔT distribution of total α events and exponential fitted function shown for crystal C6 as an example.

Table 2
Measured ^{216}Po half-lives (in ms) from exponential fit to α-α time distribution.

	Half-lives of ^{216}Po (ms)
C1	150.8 ± 4.7
C2	141.3 ± 1.5
C3	133.8 ± 5.1
C4	152.8 ± 2.6
C6	132.4 ± 4.7
C7	148.1 ± 6.8

Table 3
Measured ^{216}Po half-lives (in ms) from other sources.

	Half-lives of ^{216}Po (ms)
this work	143.4 ± 1.2
[7]	144 ± 8
[8]	144.0 ± 0.6
[9]	143.3 ± 2.8
[10]	145 ± 2
[11]	145.3 ± 18.9
global average	143.9 ± 0.5

3.3. Quenching factor calculation

The ^{220}Rn and ^{216}Po events that have been selected are shown in Fig. 5. These events were estimated using the time-delayed method outlined in Section 3.2. They are used to determine the energy-dependent quenching functions. The observed α energy and standard deviation of ^{220}Rn and ^{216}Po events are initially estimated by Gaussian fits to the identified spectral features in data. The fitted parameters are used to define the energy window applied to the α-α event selection. The energy window is set by the α energy mean plus or minus three standard deviations. A time constraint is also applied to mitigate random coincident events from ^{210}Po. From the half-life of ^{216}Po, 0.145 s, we apply a 1 s ΔT constraint.

The energy-dependent α quenching is approximated by

$$Q_\alpha(E_\alpha) = a + b \cdot E_\alpha[\mathrm{MeV}]\,, \tag{2}$$

and each data point for fitting is obtained from the ratio between the Q-value and the electron-equivalent energy of α from ^{210}Po, ^{220}Rn, and ^{216}Po. Characteristic data points and energy-dependent quenching factor functions for Q_1 and Q_2 are shown in Fig. 6. The fitted a and b parameters for each crystal are summarized in Tables 4 and 5.

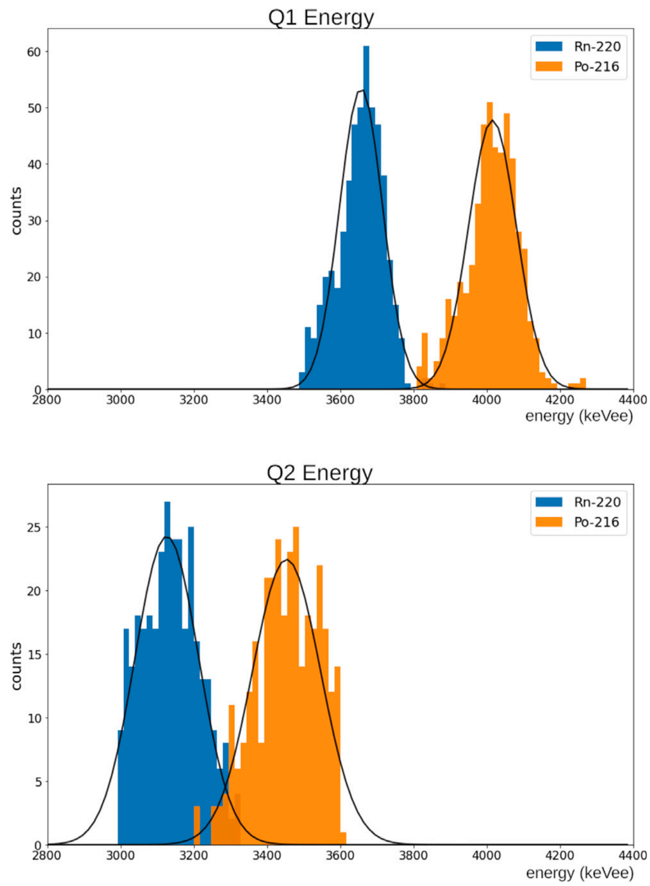

Fig. 5. Characteristic α-α electron-equivalent energy distributions of the selected ^{216}Po and ^{220}Rn events for Q_1 and Q_2 shown for crystal C6 as an example.

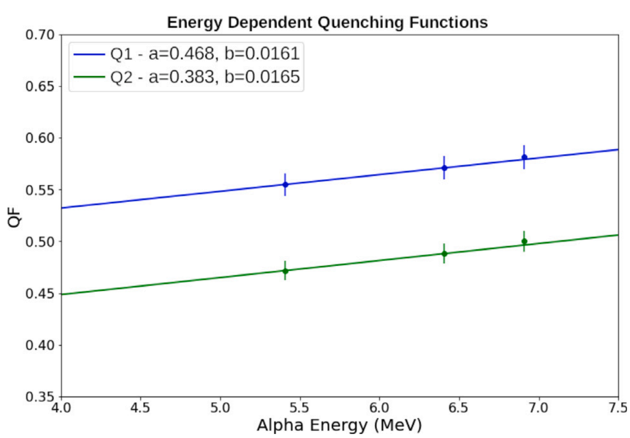

Fig. 6. Characteristic data points and energy-dependent quenching factor functions for Q_1 and Q_2 shown for crystal C6 as an example.

4. Alpha decay Monte Carlo simulation and activity determination

Radioactive background components are simulated using Geant4 (v10.4.2) [12–14]. The physics list classes of G4EmLivermorePhysics for low-energy electromagnetic processes and G4RadioactiveDecay for radioactive decay processes are used. Details of the simulation are described in Refs. [15,16].

The α events are challenging to reproduce with simulation. Two quenching factors are required to describe the two dominant α peaks from ^{210}Po as well as the higher energy features from ^{220}Rn and ^{216}Po.

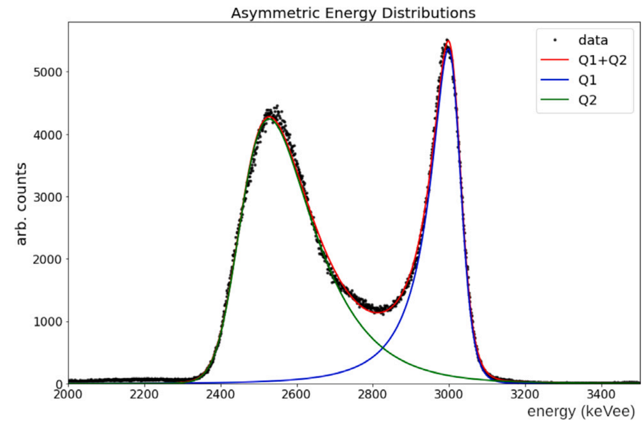

Fig. 7. Internal ^{210}Po data approximated by simulation of two quenching factors with normal-inverse Gaussian energy distributions shown for crystal C6 as an example.

Table 4
Energy-dependent Q_1 parameters as defined by Eq. (2) obtained for each crystal.

	Q_1	
	a	b
C1	0.437 ± 0.008	0.0218 ± 0.0014
C2	0.465 ± 0.008	0.0210 ± 0.0013
C3	0.419 ± 0.008	0.0242 ± 0.0014
C4	0.458 ± 0.008	0.0214 ± 0.0013
C6	0.468 ± 0.008	0.0161 ± 0.0013
C7	0.493 ± 0.007	0.0114 ± 0.0012

Table 5
Energy-dependent Q_2 parameters as defined by Eq. (2) obtained for each crystal.

	Q_2	
	a	b
C1	0.274 ± 0.011	0.0425 ± 0.0018
C2	0.415 ± 0.009	0.0216 ± 0.0014
C3	0.394 ± 0.009	0.0238 ± 0.0015
C4	0.425 ± 0.008	0.0223 ± 0.0014
C6	0.383 ± 0.009	0.0165 ± 0.0015
C7	0.399 ± 0.009	0.0135 ± 0.0015

Furthermore, the ^{210}Po spectral shapes are highly asymmetric, and an asymmetric probability density function (PDF) is required for the simulation energy smearing. One hypothesis is that the asymmetric shape is caused by spatial QF transitioning regions in the NaI(Tl) crystal. Lacking a physics explanation for the asymmetric energy distribution, a PDF was selected that closely approximated the spectral shape observed in data. In this work, the spectral shapes were approximated by the normal-inverse Gaussian [17] as demonstrated in Fig. 7.

The two prominent peaks with asymmetric spectral shape are also observed by the ANAIS experiment [5], which uses NaI(Tl) crystals produced by Alpha Spectra Inc., the same vendor that produced the crystals for COSINE-100. The ANAIS experiment cautiously proposes the lower energy peak could be due to surface ^{210}Po. We did investigate NaI(Tl) surface ^{210}Po at depths ranging from 10 μm to 10 nm using Geant4 MC simulation but could not demonstrate the large energy difference ($300-500\,keV_{ee}$) observed in data. We also investigated the effects of a scintillation dead layer [18] but could not demonstrate large energy differences. At most, energy differences while considering surface ^{210}Po and/or a dead layer were $50-100\,keV_{ee}$. We hypothesized in Section 3.1 the double peak structure could be explained by the spatial dependence of Tl doping concentration causing two quenching factors, but further investigation is needed.

The energy dependent α quenching functions determined in Section 3.3 are separately applied to the simulated α decay events to create

Table 6
Fitted fractional activities of ^{210}Po and ^{228}Th for each crystal. For other fitted isotopes, poor statistics does not allow to distinguish Q_1 and Q_2, so the fractional activities are assumed to be equal.

	^{210}Po (mBq/kg)		^{228}Th (μBq/kg)	
	Q_1	Q_2	Q_1	Q_2
C1	1.55	1.38	1.84	5.63
C2	0.48	1.38	2.10	2.46
C3	0.22	0.41	0.75	1.16
C4	0.27	0.41	1.41	1.52
C6	0.82	0.81	0.34	1.76
C7	1.01	0.62	0.41	1.73

Q_1 and Q_2 quenched energy distributions. The quenched energies are then smeared asymmetrically. The resulting simulated α spectra are in units of electron-equivalent energy and make up the templates that are fit to data. The fractional activities of the Q_1 and Q_2 templates are left as free parameters of the fit. The fitted fractional activities for ^{210}Po and ^{228}Th are listed in Table 6. For other fitted isotopes, poor statistics does not allow to distinguish Q_1 and Q_2, so the fractional activities are assumed to be equal.

4.1. Data fitting

Data are fitted by analytically maximizing the binned likelihood of two or more MC background templates as described in Ref. [19]. For each α component, MC templates are created for two quenching functions and allowed to be independently scaled by the fitting algorithm. The resulting fits to the COSINE-100 crystals are shown in Fig. 8.

The activities of less significant components of PTFE bulk ^{210}Po and NaI surface ^{210}Po are determined from analysis of the β/γ channel as presented in Ref. [16]. These background sources are included in the α background model but their activities are fixed for this work.

4.2. Spectral components

The α spectra are dominated by three distinct components. They include internal ^{210}Po (2.2–3.2 MeV$_{ee}$), internal ^{228}Th-group (3.2–4.2 MeV$_{ee}$), and PTFE surface ^{210}Po (1.0–2.2 MeV$_{ee}$). PTFE bulk ^{210}Po and NaI surface ^{210}Po are included in the background model but do not contribute significantly to the α spectrum. The activities of these components are measured in the β/γ channel and a detailed analysis is presented in Ref. [16]. The fitted activities of NaI surface ^{210}Po in the β/γ channel in crystals C1 and C4 were consistent with the null hypothesis, so this component is not included in the α spectra of C1 and C4.

4.2.1. Internal ^{210}Po

The α spectra are dominated by internal ^{210}Po at 2.2–3.2 MeV$_{ee}$. It is not understood why the ^{210}Po α energy distribution is highly asymmetric. For the purpose of this α modeling, the ^{210}Po spectral shape is parameterized by normal-inverse Gaussian distributions as this approach best approximates the shape of the ^{210}Po spectrum observed in data. Internal ^{210}Po is the dominant α background and Table 7 compares the fitted activities to measurements of the total α rates [1].

4.2.2. Internal ^{228}Th-group

The features visible at higher energies (> 3.2 MeV$_{ee}$) are dominated by internal ^{232}Th and particularly the ^{228}Th-group consisting of ^{228}Th, ^{224}Ra, ^{220}Rn, and ^{216}Po α decays. The two quenching factors (Section 3.3) are simulated and independently fit to data to determine the activity of the ^{228}Th-group. The fitted results are compared to the time-correlated α-α measurements in Table 8. The discrepancies are not well understood. It is possible an α decay isotope is not accounted for in the background model and has an energy in the region of the ^{228}Th-group causing the fit to overestimate the ^{228}Th-group activity.

Table 7
Comparison of MC fitted activity of internal ^{210}Po to the total α rate measured in Ref. [1].

	Fitted MC ^{210}Po (mBq/kg)	Total α Rate (mBq/kg)
C1	2.93 ± 0.17	3.20 ± 0.08
C2	1.86 ± 0.17	2.06 ± 0.06
C3	0.65 ± 0.10	0.76 ± 0.02
C4	0.68 ± 0.11	0.74 ± 0.02
C6	1.62 ± 0.14	1.52 ± 0.04
C7	1.63 ± 0.14	1.54 ± 0.04

Table 8
Comparison of ^{228}Th-group activity measured by fitting MC to data and by α-α coincidence as described in Section 3.2.

	Fitted MC ^{228}Th-group (μBq/kg)	α-α coinc. ^{228}Th-group (μBq/kg)
C1	7.47 ± 0.84	3.34 ± 0.94
C2	4.56 ± 0.49	3.29 ± 0.06
C3	1.91 ± 0.20	1.69 ± 0.04
C4	3.93 ± 0.21	2.25 ± 0.04
C6	2.10 ± 0.12	0.54 ± 0.02
C7	2.14 ± 0.12	0.58 ± 0.02

Table 9
PTFE surface ^{210}Po activity measured by fitting MC to data.

	PTFE Surf. ^{210}Po (μBq/cm^2)
C1	0.77 ± 0.11
C2	1.25 ± 0.13
C3	1.10 ± 0.16
C4	1.08 ± 0.12
C6	1.61 ± 0.20
C7	1.14 ± 0.13

4.2.3. PTFE surface ^{210}Po

Different α source locations and their resulting spectral shapes were studied with Geant4 simulations. From these studies, it was determined that the low-energy tail (< 2.2 MeV$_{ee}$) of the α distribution (Fig. 3) is caused by ^{210}Po on the surface of the PTFE reflector that surrounds NaI crystals. Furthermore, the depth profile of the ^{210}Po in the PTFE correlates to the slope of the low energy tail of the α distribution. A shallower depth profile causes a steeper low-energy tail. The contamination depth profiles differ among crystals and range from 2–5 μm. The fitted results are summarized in Table 9.

Using MC, we investigated the NaI surface ^{210}Pb at various depth profiles. We also investigated the effects of a scintillation dead layer [18] extending to various depths in combination with NaI surface ^{210}Pb. These scenarios did not describe the low-energy tail observed in the data.

Measurements of internal ^{210}Pb and PTFE surface ^{210}Pb half-lives were made. The measured half-life of internal ^{210}Pb was consistent with the known value of 22.3 yr while the measured half-life of PTFE surface ^{210}Pb was a much longer 33.8 ± 8.0 yr. One possible explanation is that the surface is continuously contaminated by something radioactive from outside (^{222}Rn for example) which artificially increases the observed half-life of PTFE surface^{210}Pb.

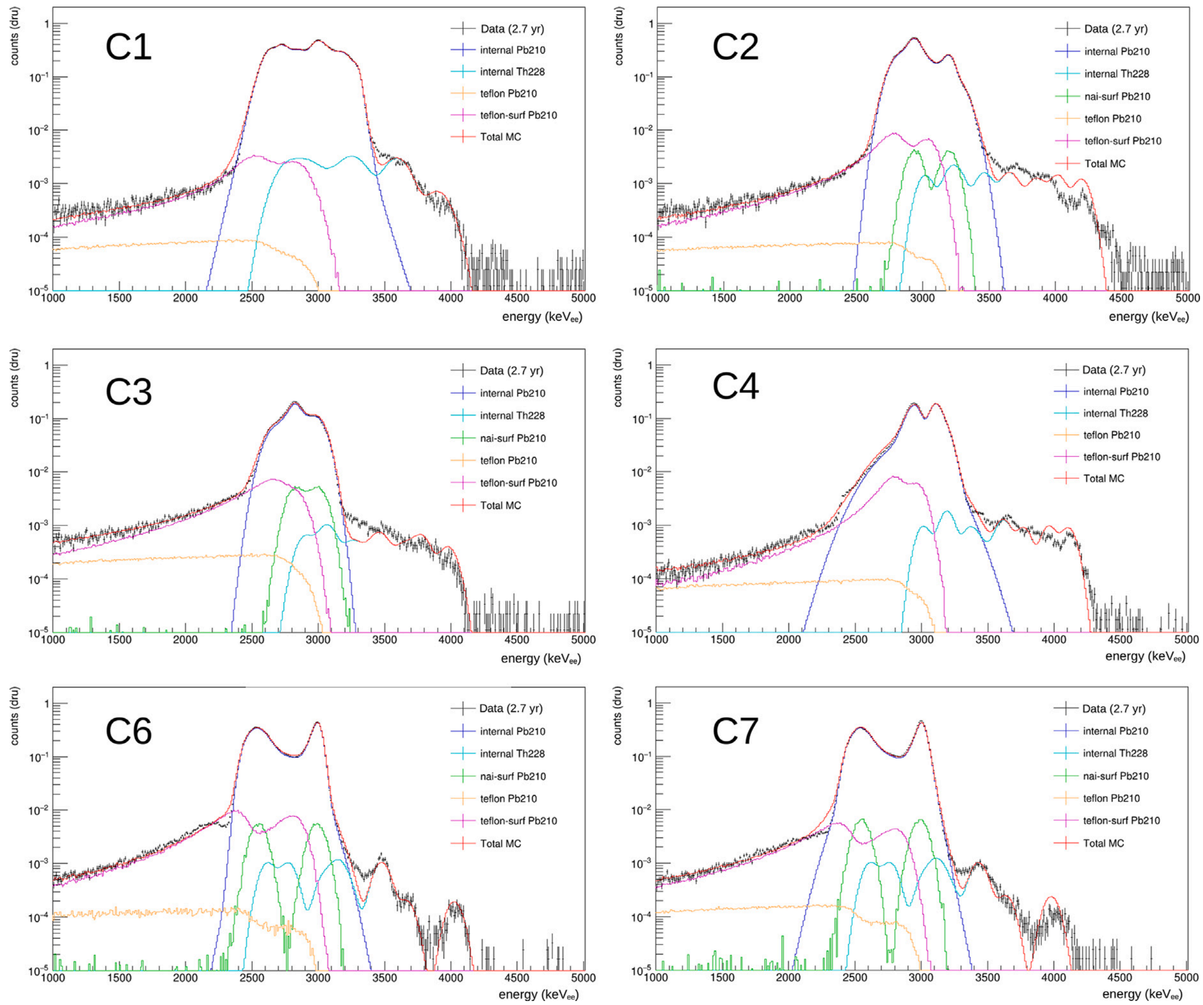

Fig. 8. Results of fitting internal ^{210}Po, internal ^{228}Th-group, and PTFE surface ^{210}Po α components to data for each COSINE-100 crystal.

5. Conclusion

Two quenching factors for alpha particles are required to describe the features in COSINE-100 data. The relative contribution of Q_1 and Q_2 is not consistent among fitted isotopes. Normal-inverse Gaussian PDFs are applied to the simulation to approximate the spectral shapes observed in α data. The two quenching factors is hypothesized by the spatial dependence of Tl concentration within the crystal effecting the quenching factor. The asymmetric spectral shape could be due to non-uniform transitions between the two quenching factors. More investigation is needed to understand these phenomena.

The COSINE-100 α spectra are well described by dominant components of internal ^{210}Po, internal ^{228}Th-group, and PTFE surface ^{210}Po. NaI surface ^{210}Po and PTFE bulk ^{210}Po activities are determined from the β/γ channel as described in Ref. [16] because their spectral features are more prominent in the β/γ channel. The α isotope activities were measured in this work by fitting Geant4 MC to data. The dominant ^{210}Po fitted α rates are consistent ($<1.1\ \sigma$) with the total α rates (Table 7), as measured during commissioning of the crystals.

Furthermore, the half-life of ^{216}Po has been measured to be 143.4 ± 1.2 ms which is consistent with and more precise than most current measurements.

CRediT authorship contribution statement

E.J. Jeon: Writing – review & editing. **M. Kauer:** Writing – review & editing, Writing – original draft, Formal analysis. **H. Lee:** Writing – review & editing. **G.H. Yu:** Writing – review & editing.

Declaration of competing interest

The authors declare that they have no known competing financial interests or personal relationships that could have appeared to influence the work reported in this paper.

Data availability

Data will be made available on request.

Acknowledgments

We thank the Korea Hydro and Nuclear Power (KHNP) Company for providing underground laboratory space at Yangyang and the IBS Research Solution Center (RSC) for providing high-performance computing resources. This work is supported by: the Institute for Basic Science (IBS) under project code IBS-R016-A1, NRF-2019R1C1C1005073, NRF-2021R1A2C3010989, NRF-2021R1A2C1013761, NFEC-2019R1A6C1010027, and NRF-2021R1I1A3041453, Republic of Korea; NSF Grants No. PHY-1913742, DGE-1122492, WIPAC, the Wisconsin Alumni Research Foundation, United States; STFC, United Kingdom Grant ST/N000277/1 and ST/K001337/1, United Kingdom; Grant No. 2021/06743-1 and 2022/12002-7 FAPESP, CAPES Finance Code 001, CNPq 131152/2020-3 and 303122/2020-0, Brazil.

References

[1] G. Adhikari, et al., Initial performance of the COSINE-100 experiment, Eur. Phys. J. C 78 (2) (2018) 107, http://dx.doi.org/10.1140/epjc/s10052-018-5590-x, arXiv:1710.05299.

[2] G. Adhikari, et al., COSINE-100 Collaboration, The COSINE-100 data acquisition system, JINST 13 (09) (2018) P09006, http://dx.doi.org/10.1088/1748-0221/13/09/P09006, arXiv:1806.09788.

[3] G. Adhikari, et al., The COSINE-100 liquid scintillator veto system, Nucl. Instrum. Methods A 1006 (2021) 165431, http://dx.doi.org/10.1016/j.nima.2021.165431, arXiv:2004.03463.

[4] H. Prihtiadi, et al., COSINE-100 Collaboration, Muon detector for the COSINE-100 experiment, JINST 13 (02) (2018) T02007, http://dx.doi.org/10.1088/1748-0221/13/02/T02007, arXiv:1712.02011.

[5] J. Amare, et al., Assessment of backgrounds of the ANAIS experiment for dark matter direct detection, Eur. Phys. J. C 76 (8) (2016) 429, http://dx.doi.org/10.1140/epjc/s10052-016-4279-2, arXiv:1604.05587.

[6] M.R. Bharadwaj, et al., Quenching Factor estimation of Na recoils in NaI(Tl) crystals using a low-energy pulsed neutron beam measurement, SciPost Phys. Proc. 12 (2023) 028, http://dx.doi.org/10.21468/SciPostPhysProc.12.028.

[7] F.A. Danevich, A.S. Georgadze, V.V. Kobychev, B.N. Kropivyansky, A.S. Nikolaiko, O.A. Ponkratenko, V.I. Tretyak, S.Y. Zdesenko, Y.G. Zdesenko, P.G. Bizzeti, T.F. Fazzini, P.R. Maurenzig, Search for 2β decay of cadmium and tungsten isotopes: Final results of the Solotvina experiment, Phys. Rev. C 68 (2003) 035501, http://dx.doi.org/10.1103/PhysRevC.68.035501, URL https://link.aps.org/doi/10.1103/PhysRevC.68.035501.

[8] L. Nadderd, K. Subotić, Y. Tsyganov, J. Puzović, A. Polyakov, A. Rykhlyuk, D. Manić, Measurement of the life-times distribution of 216Po, Nucl. Instrum. Methods Phys. Res. A 868 (2017) 119–121, http://dx.doi.org/10.1016/j.nima.2017.06.055, URL https://www.sciencedirect.com/science/article/pii/S0168900217307088.

[9] O. Azzolini, et al., Measurement of 216Po half-life with the CUPID-0 experiment, Phys. Lett. B 822 (2021) 136642, http://dx.doi.org/10.1016/j.physletb.2021.136642, URL https://www.sciencedirect.com/science/article/pii/S0370269321005827.

[10] H. Diamond, J. Gindler, Alpha half-lives of 216Po, 217At and 218Rn, J. Inorg. Nucl. Chem. 25 (2) (1963) 143–149, http://dx.doi.org/10.1016/0022-1902(63)80001-9, URL https://www.sciencedirect.com/science/article/pii/0022190263800019.

[11] G. Baccolo, A. Barresi, M. Beretta, D. Chiesa, M. Nastasi, L. Pagnanini, S. Pozzi, E. Previtali, M. Sisti, G. Terragni, Improving radioactive contaminant identification through the analysis of delayed coincidences with an α-spectrometer, Eur. Phys. J. C 81 (11) (2021) 971, http://dx.doi.org/10.1140/epjc/s10052-021-09759-5, arXiv:2105.03140.

[12] S. Agostinelli, et al., GEANT4 Collaboration, GEANT4–A simulation toolkit, Nucl. Instrum. Methods A 506 (2003) 250–303, http://dx.doi.org/10.1016/S0168-9002(03)01368-8.

[13] J. Allison, et al., Geant4 developments and applications, IEEE Trans. Nucl. Sci. 53 (2006) 270, http://dx.doi.org/10.1109/TNS.2006.869826.

[14] J. Allison, et al., Recent developments in Geant4, Nucl. Instrum. Methods A 835 (2016) 186–225, http://dx.doi.org/10.1016/j.nima.2016.06.125.

[15] G. Adhikari, et al., Understanding NaI(Tl) crystal background for dark matter searches, Eur. Phys. J. C 77 (7) (2017) 437, http://dx.doi.org/10.1140/epjc/s10052-017-5011-6, arXiv:1703.01982.

[16] P. Adhikari, et al., COSINE-100 Collaboration, Background model for the NaI(Tl) crystals in COSINE-100, Eur. Phys. J. C 78 (2018) 490, http://dx.doi.org/10.1140/epjc/s10052-018-5970-2, arXiv:1804.05167.

[17] O. Barndorff-Nielsen, Exponentially decreasing distributions for the logarithm of particle size, Proc. R. Soc. Lond. Ser. A 353 (1674) (1977) 401–419, URL http://www.jstor.org/stable/79167.

[18] P. Yang, C.D. Harmon, F.P. Doty, J.A. Ohlhausen, Effect of Humidity on Scintillation Performance in Na and Tl Activated CsI Crystals, IEEE Trans. Nucl. Sci. 61 (2) (2014) 1024–1031, http://dx.doi.org/10.1109/TNS.2014.2300471.

[19] R.J. Barlow, C. Beeston, Fitting using finite Monte Carlo samples, Comput. Phys. Comm. 77 (1993) 219–228, http://dx.doi.org/10.1016/0010-4655(93)90005-W.